Interlaminar Tension Strength of Graphite/Epoxy Composite Laminates

Kunigal N. Shivakumar,* Harold G. Allen,† and Vishnu S. Avva‡
North Carolina A & T State University, Greensboro, North Carolina 27411

An L-shaped curved beam specimen and a tension loading fixture were proposed to measure the interlaminar tension strength of laminated and textile composites. The specimen size was 2 × 2 in. (51 × 51 mm). The use of a standard tension test machine and the introduction of load nearly at the specimen midthickness were the advantages of the proposed specimen. Modified Lekhnitskii and beam theory equations for calculating interlaminar stresses of an L-beam were verified by finite element analysis. The beam theory equation is simple and accurate for mean radius to thickness ratios greater than 1.5. The modified Lekhnitskii equations can be used for detailed stress field calculation. AS4/3501-6 graphite/epoxy unidirectional specimens with thicknesses of 16, 24, and 32 plies were fabricated and tested. The delamination initiation site agreed with the calculated maximum interlaminar tension stress location for all three thicknesses. Average interlaminar tension strengths of 16-, 24-, and 32-ply laminates were 47.6, 40.9, and 23.4 MPa, respectively. Results of 16- and 24-ply specimens agreed reasonably well with data in literature for a longer size specimen and a different loading fixture. Interlaminar tension strength decreased with increased specimen thickness and width because of volumetric effect.

Introduction

TEST methods for measuring in-plane strengths—longitudinal, transverse, and shear strengths—are well established, and the procedures are well documented in the American Standard for Testing and Materials handbook. However, no standard has been developed to measure the interlaminar tension strength of laminated composite materials. Interlaminar tension strength is an important parameter in design of structures subjected to out-of-plane loads, structural joints, attachments, etc. Several attempts have been made in the literature to measure the transverse tension strength, also referred to as the interlaminar tension strength, of laminates and to establish a test specimen and the procedure. The two types of specimens used were a 90-deg laminate tension specimen[1-3] and a curved beam specimen.[4-9] The transverse tension specimen had a number of drawbacks, including the quality of fabrication, applying uniform stress, and stress concentration due to specimen taper. Because of differences in fabrication process and triaxial stress constraint in the transverse tension specimen and structural components, the transverse strength measured from the tension specimen may be different from the interlaminar tension strength of structural components.

After Ko and Jackson[4] showed that thick curved multilayer composite specimens develop interlaminar tension (radial) stresses that are high enough to cause the transverse failure of laminates, curved beam specimens were proposed.[4-9] Two types of curved beam specimens were used in the literature, namely, C-beam[4-7] and L-beam.[8,9] These specimens with different types of loading arrangement were used to measure the transverse strength (delamination onset) and delamination growth of laminated composites. Although test specimens were successful to a varied degree, the problem of load introduction and specimen size were not addressed satisfactorily. The specimen sizes of textile composites are restricted by the braiding man-

drel or the weaving machine. To use the same size specimen for laminated as well as textile composites, the specimen size in this study was restricted to about 2 in. (51 mm).

Objectives of this paper are to develop a 2 × 2 in. L-beam specimen with an appropriate load fixture so that it can be tested in a standard tension test machine and a simple equation to calculate the interlaminar tension strength from the measured failure load and specimen configuration. The proposed specimen is an L-beam with arm lengths of 2 in. (51 mm) and an inner radius at the curved section of 0.25 in. (6.4 mm). This specimen is similar to the one that was proposed in Ref. 9, but with a shorter length. As mentioned previously, the arm length was selected based on the fabrication restriction of textile composite materials.

The L-beam specimen's configuration and fabrication procedure and the load fixture are described. Three laminate thicknesses, namely, 16, 24, and 32 ply, were fabricated and tested. Finite element analysis is conducted, and modified Lekhnitskii[10] and beam theory equations are derived for the L-beam. The interlaminar transverse tension strength of AS4/3501-6 unidirectional graphite/epoxy laminates are calculated. The results are compared with those reported in literature for different specimen configurations.

Specimen Configuration and Loading Fixture

Test Specimen

The proposed equal leg-length L-beam specimen is shown schematically in Fig. 1. The specimen length is about 2 in. (51 mm); this length was determined based on the size restriction
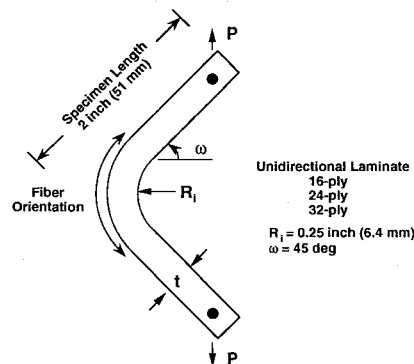

Fig. 1 Specimen configuration.

of textile composites. The inner radius R_i of the beam at the curved section is 0.25 in. (6.4 mm). The specimen width w is 1.5 in. (38.1 mm). Three thicknesses t were chosen, namely, 16, 24, and 32 plies. The outer radius of the beam is $R_o = R_i + t$. The material is the AS4/3501-6 graphite/epoxy composite with lamina properties:

$$E_{\theta\theta}(E_{ll}) = 19 \text{ Msi (131 GPa)} \qquad E_{rr}(E_{tt}) = 1.89 \text{ Msi (13 GPa)}$$

$$G_{\theta r}(G_{lt}) = 0.93 \text{ MSI (6.4 GPa)} \qquad \nu_{\theta r}(\nu_{lt}) = 0.34$$

where subscripts l and t refer to longitudinal and transverse directions of the fibers, respectively. Subscripts r and θ refer to radial and tangential directions at the curved section of the beam. The unidirectional laminated specimen was selected to prevent matrix cracks and edge delaminations.

The curved laminated specimen was fabricated by laying up 12-in. (305-mm) strips of unidirectional plies over the corner of a solid rectangular aluminum mold. The radius of the corner was 0.25 in. (6.4 mm). Each of the straight arms was about 2.5 in. (64 mm) long. The stacked plies and the mold were vacuum bagged and cured in autoclave according to the material manufacturers' specifications. Details of the specimen fabrication are given in Ref. 11. Specimens were then machined to 1.5 in. (38 mm) wide and 2 in. (51 mm) long from the 12 × 2.5 in. (305 × 64 mm) laminate. The two edges of the specimen were polished, and the exact width and the thickness were measured using a caliper. Specimen edges were painted white with a water-based typewriter correction fluid to identify the location of the transverse tension failure. Five specimens were manufactured for each of the three thicknesses.
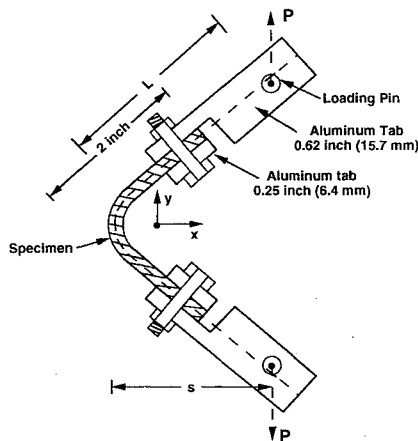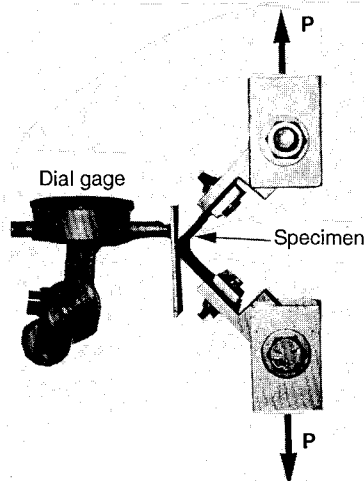

Fig. 2 Specimen loading fixture.

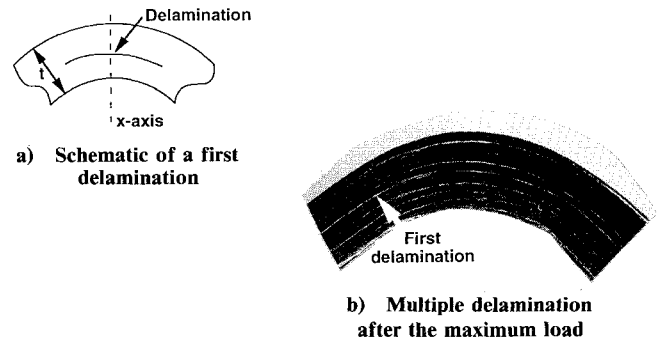
Fig. 3 Specimen and the loading fixture.

a) Schematic of a first delamination

b) Multiple delamination after the maximum load

Fig. 4 Single and multiple delaminations.

Loading Fixture

A special load fixture was fabricated so that the specimen could be tested in a standard tension test machine, and the load was introduced nearly at the midthickness of the specimen. Figure 2 shows schematically the specimen attachment fixture. Ends of the specimen were clamped using two reusable aluminum tabs and two 0.25-in. (6.4-mm) high-strength bolts. The two bolts were spaced 0.75 in. (19 mm) apart in the width direction and were tightened to about 50-in.-lb torque. The thickness of the top tab at the loading end was more than the sum of the thicknesses of the two tabs at the bolted end and the specimen (about 25 mm). The specimen was loaded through a 0.5-in. (13-mm) diam steel pin, which was attached to the test machine through a U-type universal joint (see Fig. 3). Note that in every test the distance s between the load axis and the outer edge of the specimen is measured. The value of s is then used in Eq. (1) to calculate the loading arm length L,

$$L = \frac{s - t/2 + R_m(1 - \sin \omega)}{\cos \omega} \qquad (1)$$

where ω is the inclination of the loading arm with the x axis (see Fig. 2); in the present case $\omega = 45$ deg. The mean radius R_m is $(R_i + R_o)/2$. Note that the length L includes the specimen arm and the loading fixture (see Fig. 2). Because the stress boundary-value analysis was used in calculating the stresses at the curved section of the specimen, the material properties within the length L have no impact on the results.

Test Procedure and Results

The specimen and the loading fixture assembly (see Fig. 3) were mounted on a servohydraulically controlled tension test machine. A small preload (about 5 lb) was applied on the specimen to measure the distance between the load axis and outer edge of the specimen, s (see Fig. 2). This procedure was repeated for all specimens. The measured value of s was used in analytical modeling of the specimen and the loading fixture. Tests were conducted under displacement controlled at 1 mm/min. The load and displacements were digitally recorded. The interlaminar tension failure load was recorded when a sudden decrease in load occurred; the load drop was accompanied by a loud "pop" noise. The load drop was more than 20% of the peak load for most of the specimen. The load at the incipient of delamination represented the transverse tension failure load, and it was used in calculating the interlaminar tension strength. Observation on edges of the specimen showed a delamination near the midthickness of the specimen (see Fig. 4a), where the transverse tension stress was highest. Subsequent loading on the specimen showed multiple steps of load decreases associated with the development of multiple delaminations on either side of the initial delamination. A micrograph of a typical 24-ply specimen is shown in Fig. 4b. All fifteen specimens were tested, and the load displacements were recorded.

Figures 5–7 show the load-displacement curves for 16-, 24-, and 32-ply laminates. Because the preload was applied before the displacement was started recording, the load-displacement
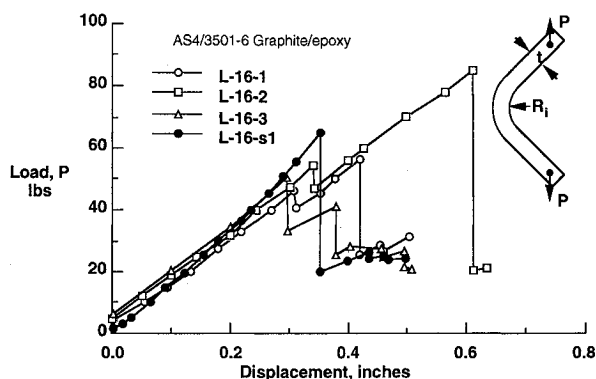
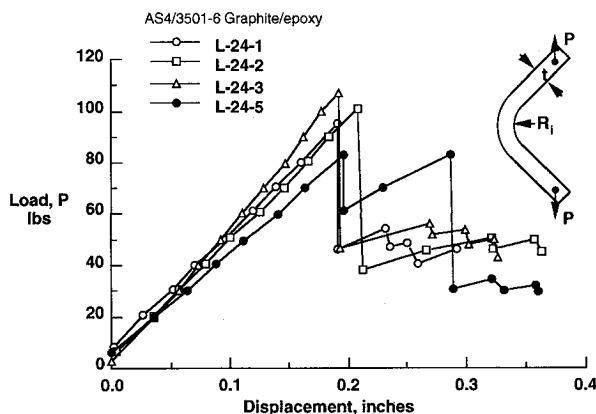Fig. 5   Load-displacement plot of 16-ply-thick specimens.

Fig. 6   Load-displacement plot of 24-ply-thick specimens.

curves show an initial load offset. To improve the clarity of figures, only four specimen data are shown for each of the three thicknesses. Initiation of interlaminar tension failure is shown by a sudden drop in the load. The load at the incipient of the transverse tension failure was the largest value, and the specimen did not bear a load larger than this value until the specimen started straightening. The failure load was used in the analysis to calculate the interlaminar tension strength. The distance between the delamination initiation site and the inner surface of the beam ranged from $0.41t$ to $0.49t$ for the 16-ply specimen, $0.38t$ to $0.49t$ for the 24-ply specimen, and $0.40t$ to $0.46t$ for the 32-ply specimen. The mean values were $0.45t$, $0.44t$, and $0.43t$ for 16-, 24-, and 32-ply specimens, respectively. In Table 1, the delamination initiation site is compared with the maximum radial stress location from various analyses.

The load-displacement curves for the 32-ply laminate showed nonlinear response due to initiation of premature failures at resin-rich pockets. The quality of the 32-ply laminates was poor compared with that of the 16- and 24-ply laminates. Molding of the 32-ply laminate took more time, and it was difficult. While molding the laminate, each ply at a time, ply crimps and waviness were almost unavoidable after molding about 25 plies. These crimps and waviness contributed to the development of resin-rich pockets. No such problems were encountered in fabricating 16- and 24-ply laminates.

Analysis

Two-dimensional finite element (F-E) analysis, Lekhnitskii[10] solution with a superposition principle, and a beam theory equation were used to calculate the stress field on the symmetric axis of the L-beam. The F-E analysis was conducted using an in-house finite element code FEM2D8. Calculated radial and tangential stresses from various analyses were compared with each other.

Finite Element Analysis

An in-house two-dimensional finite element code FEM2D8, based on an eight-node isoparametric element, was used to conduct the stress analysis of the L-beam specimen and the loading fixture. The loading fixture was idealized as an equivalent arm, and the length L was calculated from the measured value of s. Because the specimen and the loading were symmetric, only the top half of the specimen was modeled. The mesh idealization had 15 elements through the thickness and one element at every one degree in the circumferential direction. A transition was made to a coarse mesh to model the straight loading arm (see Fig. 8). The model had 945 elements, 2992 nodes, and 5984 degrees of freedom. The load P was applied at the right end and midthickness of the model. The symmetry boundary condition on $y = 0$ plane and zero x displacement at the load point were imposed. The plane-stress analysis was conducted by setting the load P to unity. Calculated stresses were scaled by the failure load measured in the test. The analysis was repeated for all specimens using the measured values of the laminate thickness and s. Because the deflection at the incipient of the transverse tension failure was small, the effect of large deflections was neglected.

Modified Lekhnitskii Solution

The Appendix summarizes expressions for radial, tangential, and shear stresses for a cylindrical orthotropic circular
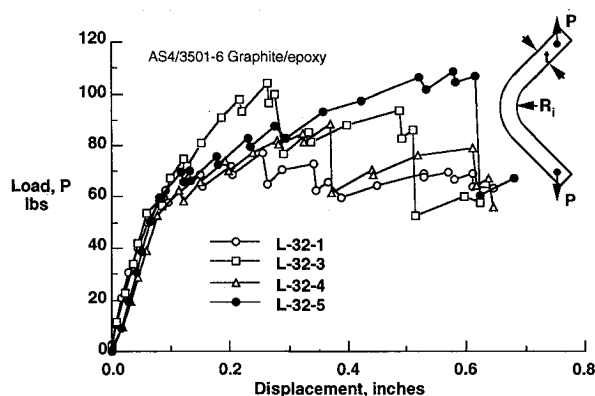

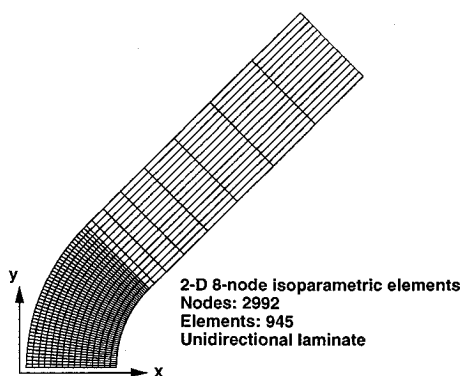Fig. 7   Load-displacement plot of 32-ply-thick specimens.

Fig. 8   Finite element idealization of symmetric top half of the L-beam (note that only part of the specimen arm is shown).

Table 1   Location of maximum radial stress and delamination initiation site

Number of plies	Location of maximum radial stress $(r - R_i)/t$			Location of delamination initiation $[(r - R_i)/t]^a$
	F-E analysis	Lekhnitskii	Beam	
16	0.47	0.45	0.47	0.45
24	0.40	0.40	0.45	0.44
32	0.40	0.40	0.43	0.43

[a]Average of three specimen data.

beam subjected to bending moment M (see Fig. 9a) and end load P (see Fig. 9b). The end load solution presented is for a semicircular beam. The bending solution is valid for both part circular and semicircular beams. These two sets of solutions and the superposition principle were used to derive radial and tangential stress equations for an L-beam. Figure 10 presents a sequence of superposition steps involved in transforming the end load on the L-beam to a semicircular beam. The first step was to transform the load P at the ends of the L-beam to the ends of the quarter circular beam as a load P and moment Mp. The second step was to transform load P from the ends of the quarter circular beam to a semicircular beam, for which all solutions are presented in the Appendix, as an end load P and the moment Mc (see Fig. 10c). Finally, in Fig. 10d the two moments Mp and Mc are summed, $M = Mp + Mc$. The solution to the L-beam with an end load P reduces to the solution of a semicircular beam subjected to the end load P and the moment M. The expression for M is given by

$$M = P(L \cos \omega - R_m \sin \omega) \tag{2}$$

The expression for L is given in Eq. (1). Since stresses are maximum along the symmetric axis, in Eqs. (A5) and (A6) $\theta = 90$ was substituted. Then expressions for radial and tangential stresses due to M and P are given by

$$\sigma_r = \sigma_r^m + \sigma_r^p \tag{3}$$

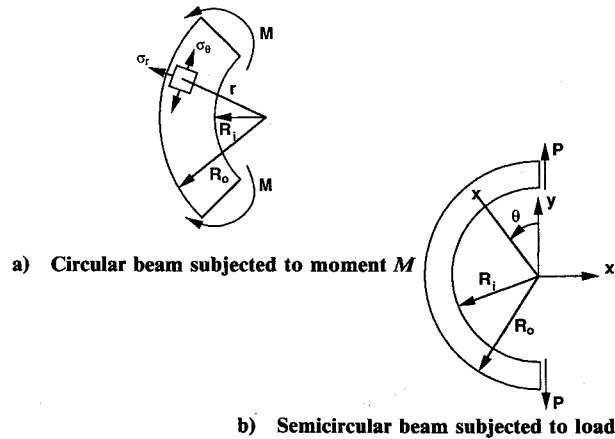$$\sigma_\theta = \sigma_\theta^m + \sigma_\theta^p \tag{4}$$

a) Circular beam subjected to moment M

b) Semicircular beam subjected to load P

Fig. 9 Cylindrically orthotropic beam subjected to moment and end load.

a) Specimen and loading

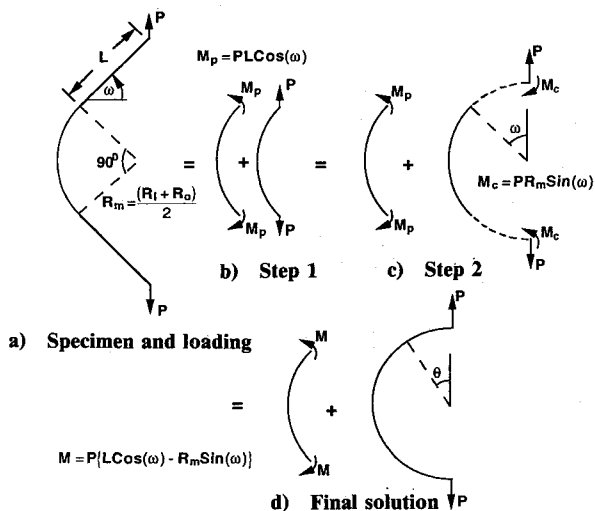b) Step 1   c) Step 2

d) Final solution

Fig. 10 Superposition of loads to derive the Lekhnitskii solution for an L-beam.
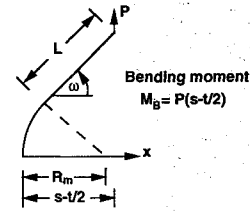

Fig. 11 Free body diagram of a symmetric half of the L-beam.
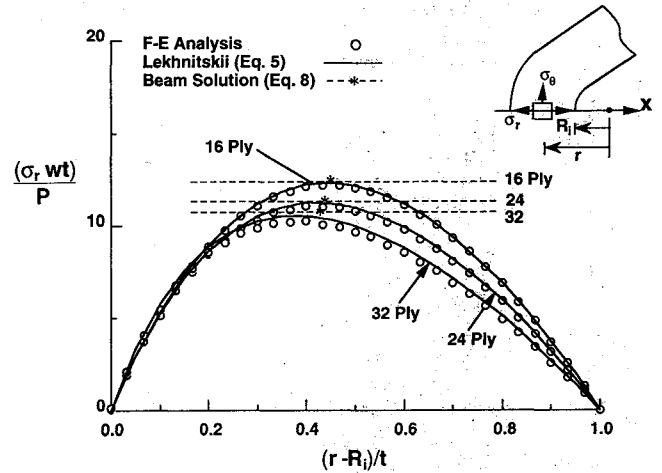

Fig. 12 Distribution of normalized radial stress through the thickness of the specimen.

Substituting radial and tangential stress expressions for bending and end loads in Eqs. (3) and (4) using Eqs. (A1), (A2), (A5), and (A6), and substituting for M from Eq. (2), results in

$$\sigma_r = -\frac{P(L \cos \omega - R_m \sin \omega)}{R_o^2 wg} \left[1 - \frac{1 - \rho^{\kappa+1}}{1 - \rho^{2\kappa}} \left(\frac{r}{R_o}\right)^{\kappa-1} \right.$$
$$\left. - \frac{1 - \rho^{\kappa+1}}{1 - \rho^{2\kappa}} \rho^{\kappa+1} \left(\frac{R_o}{r}\right)^{\kappa+1} \right]$$
$$+ \frac{P}{rwg_1} \left[\left(\frac{r}{R_o}\right)^\beta + \rho^\beta \left(\frac{R_o}{r}\right)^\beta - 1 - \rho^\beta \right] \tag{5}$$

$$\sigma_\theta = -\frac{P(L \cos \omega - R_m \sin \omega)}{R_o^2 wg} \left[1 - \frac{1 - \rho^{\kappa+1}}{1 - \rho^{2\kappa}} \kappa \left(\frac{r}{R_o}\right)^{\kappa-1} \right.$$
$$\left. + \frac{1 - \rho^{\kappa-1}}{1 - \rho^{2\kappa}} \kappa \rho^{\kappa+1} \left(\frac{R_o}{r}\right)^{\kappa+1} \right] + \frac{P}{rwg_1} \left[(1 + \beta)\left(\frac{r}{R_o}\right)^\beta \right.$$
$$\left. + (1 - \beta)\left(\frac{R_o}{r}\right)^\beta \rho^\beta - 1 - \rho^\beta \right] \tag{6}$$

Radial and tangential stresses for various L-beam configurations were calculated and compared with F-E and beam solutions.

Beam Theory Solution

Kedward et al.[7] proposed a modified elementary beam theory of isotropic materials to determine the maximum radial stress in a circular curved beam subjected to pure bending. Although this theory does not account for the material anisotropy, results were found to be valid for many of the composite materials that are currently being used. The analysis was based on the assumption that the tangential stress varies linearly through the thickness and the maximum radial stress occurs on the radial distance $\sqrt{R_i R_o}$. In the L-specimen considered, the maximum bending moment occurs on the symmetric x axis of the beam. Bending moment M_B, calculated from the free body diagram (middle surface of the beam) shown in Fig. 11, is

$$M_B = P(s - t/2) \tag{7}$$

Neglecting the effect of axial force P at the symmetric axis, the maximum radial stress is expressed as

$$(\sigma_r)_{max} = \frac{3P(s - t2)}{2wt\sqrt{R_iR_o}} \quad (8)$$

The location of the maximum stress, calculated from the expression $\sqrt{R_iR_o}$, is at $0.47t$, $0.45t$, and $0.43t$ for 16-, 24-, and 32-ply laminates, respectively.

Analytical Results

Figure 12 shows distribution of normalized radial tension stress along the x axis for 16-, 24-, and 32-ply laminates. The ordinate represents the radial stress σ_r normalized by the average stress (P/wt). The abscissa represents the normalized radial distance measured from the inner surface of the specimen. The value of $(r - R_i)/t$ varies between zero and one, representing the region between inner and outer surfaces of the curved section of the beam. Finite element results are shown by circular symbols, the modified Lekhnitskii solution by solid curves, and the beam theory solution by horizontal dash curves. Since the beam solution gave only the maximum stress, it is shown by the symbol * and dashed horizontal line. All three solutions agree very well. The largest difference between the beam and Lekhnitskii solutions is 1.5% for the 32-ply laminate $(R_m/t = 1.75)$. The largest difference between the finite element and Lekhnitskii solutions is about 3%; it is also for the 32-ply laminate. The difference is less than 1% for 16- and 24-ply laminates. Therefore the radial stress equation (5) derived from the fundamental solutions of Lekhnitskii is accurate. Figure 13 shows a comparison of the beam solution [Eq. (8)] with the modified Lekhnitskii solution [Eq. (5)] for calculating the radial stress σ_r. The difference between the two solutions is less than 2% for $R_m/t > 1.5$. A similar conclusion was arrived at in Ref. 7 for a C-beam specimen. Therefore,
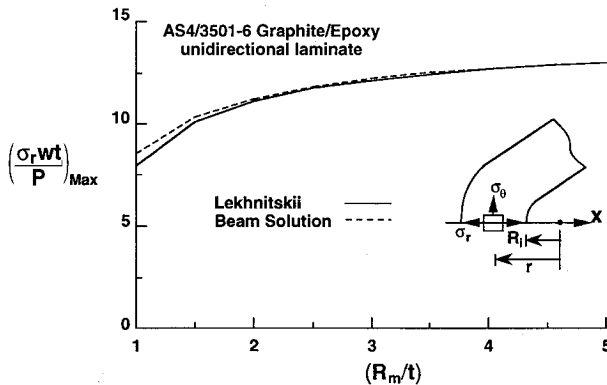

Fig. 13 Comparison of maximum radial stress calculated from beam solution with Lekhnitskii solution for various values of R_m/t ratios.
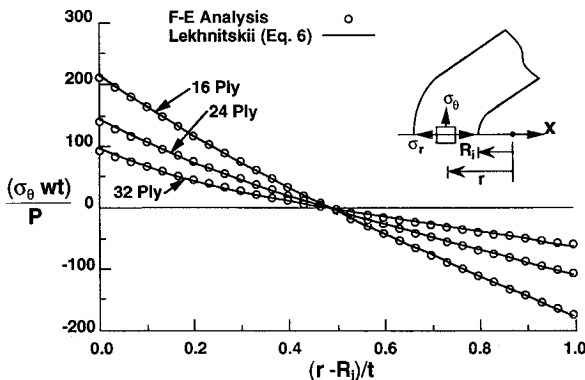

Fig. 14 Variation of normalized tangential stress through the thickness of the specimen.
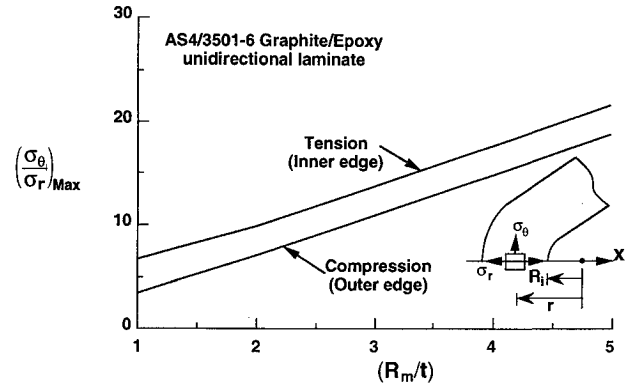

Fig. 15 Variation of ratio of maximum tangential stress and maximum radial stress with R_m/t ratio.
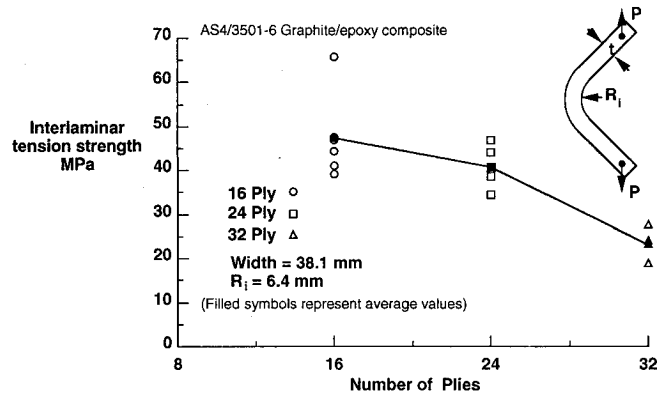

Fig. 16 Variation of interlaminar tension strength with specimen thickness.

Eq. (8) is used in the present study to calculate the interlaminar tension strength.

The locations of maximum stresses calculated from the three analyses are tabulated in Table 1, and they agree reasonably well. This table also lists measured locations of delamination initiation sites for all three specimen thicknesses. Test results were the mean of three specimen data. The location of maximum radial stress and the delamination initiation sites agree reasonably well.

Variation of tangential stress σ_θ along the x axis is shown in Fig. 14. Tangential stress varied nonlinearly through the thickness and has the maximum value at the inner surface of the curved beam. Finite element and modified Lekhnitskii solutions agree very well for all three laminates. The maximum difference between the two methods is about 3%; it is for the 32-ply laminate.

The ratio of maximum radial to tangential stress is 0.06, 0.08, and 0.11 for 16-, 24-, and 32-ply laminates, respectively. A decrease in ratio of radial to tangential stresses with decrease in the laminate thickness indicates a less likelihood of transverse tension failure in specimens thinner than 16 plies. Therefore, a thin L-beam (less than 16 ply) may not fail in transverse tension. In contrast, laminates thicker than 16 plies fail by interlaminar tension. Figure 15 shows a variation of the ratio of maximum tangential stress and maximum radial stress with R_m/t ratio. The tangential stress is tensile at the inner edge of the beam, and it is compression at the outer edge. This plot can be used to design an L-beam specimen so that interlaminar tension failure occurs in the specimen, instead of in-plane tension or the compression failure.

Interlaminar Tension Strength

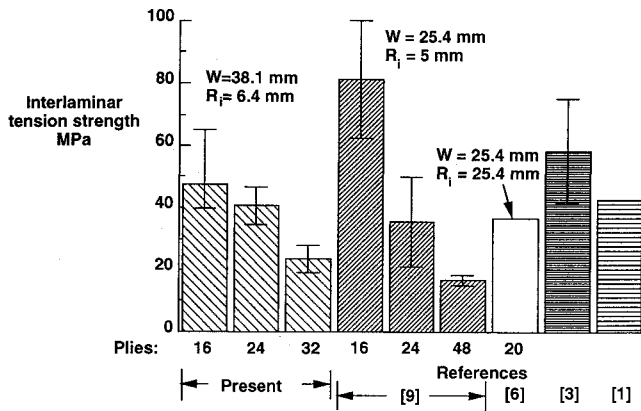Interlaminar tension strengths of all specimens were calculated from the measured failure load and Eq. (8). Calculated

Fig. 17 Comparison of present interlaminar tension strength with data reported in literature.

strength values for 16-, 24-, and 32-plies are shown in Fig. 16. Five specimen data for each thickness are presented. The solid symbol represents the average value, and it is 47.6, 40.9, and 23.4 MPa for 16-, 24-, and 32-ply laminates, respectively. The decrease in strength with the thickness is because of high probability of having more number and larger size of defects in a large volume of material. Thus a thick specimen would fail at a lower stress than a thin specimen subjected to a similar stress state. The difference in measured strengths of 16- and 24-ply laminates is due to the volume effect. In the case of the 32-ply laminates, as previously explained, the poor quality of fabrication also contributed to the lower strength. Therefore, when thick sections are used in structural applications, L-beams of appropriate thickness need to be fabricated and the strength measured.

Figure 17 compares the interlaminar tension strengths from the present study with data from Refs. 1, 3, 6, and 9. Data in Ref. 3 were for a 90-deg specimen, Ref. 1 was for a through-the-thickness tension specimen, Ref. 6 was for a C-beam specimen, and Ref. 9 was for a long L-beam specimen (25.4 mm wide and 80 mm). The loading arrangement in Ref. 9 was different from the one that was used in the present study. The data presented in the figure encompass the effect of specimen thickness, width, and type. Interlaminar strength of the 24-ply specimen from the present study (40.9 MPa) agreed well with data in Refs. 1 (43.0 MPa), 6 (36.9 MPa), and 9 (35.8 MPa), though the widths and specimen types were different. The specimen width in Refs. 6 and 9 was 25.4 mm. The strength of the 24-ply specimen was about 25% smaller than the transverse tension specimen data, 57.6 MPa.[3] The strength of the 16-ply specimen from the present study was smaller than in Ref. 9. Reference 9 reports that the average strength of the 12.7- and 25.4-in.-wide specimens was the same as that of the 16-ply specimens and differed significantly (about 37%) for the 24-ply specimens. Therefore, some of the reasons for the difference between the present data and Ref. 9's data for 16-ply specimens may be due to width effect and anticlastic bending[12] induced stresses near the free edges of the wider specimen (large w/t ratio). The average strength of 32- and 48-ply specimens is 23.4 and 17.0 MPa. Unfortunately the quality of both specimens was poor due to resin rich pockets introduced during the fabrication.

Concluding Remarks

An equal leg L-shaped curved beam specimen and a tension loading fixture were proposed to measure the interlaminar tension strength of laminated and textile composites. The specimen size was 2 × 2 in. (51 × 51 mm). The use of a standard tension test machine and the introduction of load nearly at the specimen midthickness were the advantages of the proposed specimen. Modified Lekhnitskii and beam theory equations for calculating the interlaminar stresses of an L-beam were verified by a two-dimensional finite element analysis. The

beam theory equation is simple and accurate for a mean radius to thickness ratio greater than 1.5. The modified Lekhnitskii equations gave the complete stress field at the curved section of the beam. AS4/3501-6 graphite/epoxy unidirectional specimens with thicknesses of 16, 24, and 32 plies were fabricated and tested. The delamination initiation site agreed with the calculated maximum interlaminar tension stress location for all three specimen thicknesses. Measured interlaminar tension strengths of 16-, 24-, and 32-ply laminates were 47.6, 40.9, and 23.4 MPa, respectively. Results of 16- and 24-ply specimens agreed reasonably well with data in literature for a longer size specimen and different loading fixture. Interlaminar tension strength decreased with increased specimen thickness and width. The decrease in strength with the thickness is because of the high probability of having more number and larger size of defects in a large volume of material.

Appendix: Lekhnitskii Solution for a Cylindrically Orthotropic Curved Beam

The classical elasticity theory equations for stresses in a cylindrically orthotropic homogeneous curved beam subjected to bending moment M and end load P are given in Lekhnitskii's book.[10] Expressions for radial σ_r, tangential σ_θ, and shear stresses $\tau_{r\theta}$ for plane stress condition are summarized here. In the case of end loading, the beam is considered to be semicircular. The loading and the geometric configuration of the model are shown in Fig. 9.

A. Stresses Due to Pure Bending Moment M

$$\sigma_r^m = -\frac{M}{R_o^2 wg}\left[1 - \frac{1-\rho^{\kappa+1}}{1-\rho^{2\kappa}}\left(\frac{r}{R_o}\right)^{\kappa-1}\right.$$
$$\left. -\frac{1-\rho^{\kappa-1}}{1-\rho^{2\kappa}}\rho^{\kappa+1}\left(\frac{R_o}{r}\right)^{\kappa+1}\right] \tag{A1}$$

$$\sigma_\theta^m = -\frac{M}{R_o^2 wg}\left[1 - \frac{1-\rho^{\kappa+1}}{1-\rho^{2\kappa}}\kappa\left(\frac{r}{R_o}\right)^{\kappa-1}\right.$$
$$\left. +\frac{1-\rho^{\kappa-1}}{1-\rho^{2\kappa}}\kappa\rho^{\kappa+1}\left(\frac{R_o}{r}\right)^{\kappa+1}\right] \tag{A2}$$

$$\tau_{r\theta}^m = 0 \tag{A3}$$

where

$$\kappa = \sqrt{\frac{E_\theta}{E_r}}, \qquad \rho = \frac{R_i}{R_o}$$

and

$$g = \frac{1-\rho^2}{2} - \frac{\kappa}{\kappa+1}\frac{(1-\rho^{\kappa+1})^2}{1-\rho^{2\kappa}} + \frac{\kappa\rho^2}{\kappa-1}\frac{(1-\rho^{\kappa-1})^2}{1-\rho^{2\kappa}}$$

The maximum radial stress occurs at the radial distance

$$(r)_{max}^M = \left[\frac{(\kappa+1)(1-\rho^{\kappa-1})\rho(R_iR_o)^\kappa}{(\kappa-1)(1-\rho^{\kappa+1})}\right]^{\frac{1}{2\kappa}} \tag{A4}$$

B. Stresses Due to End Load P

$$\sigma_r^P = \frac{P}{Rwg_1}\left[\left(\frac{r}{R_o}\right)^\beta + \rho^\beta\left(\frac{R_o}{r}\right)^\beta - 1 - \rho^\beta\right]\sin\theta \tag{A5}$$

$$\sigma_\theta^P = \frac{P}{Rwg_1}\left[(1+\beta)\left(\frac{r}{R_o}\right)^\beta + (1-\beta)\left(\frac{R_o}{r}\right)^\beta\rho^\beta - 1 - \rho^\beta\right]\sin\theta \tag{A6}$$

$$\tau_{r\theta}^P = \frac{P}{Rwg_1}\left[\left(\frac{r}{R_o}\right)^\beta + \rho^\beta\left(\frac{R_o}{r}\right)^\beta - 1 - \rho^\beta\right]\cos\theta \tag{A7}$$

where

$$\beta = \sqrt{1 + \frac{E_\theta}{E_r}(1 - 2\nu_{r\theta}) + \frac{E_\theta}{G_{r\theta}}}$$

and

$$g_1 = \frac{2}{\beta}(1 - \rho^\beta) + (1 + \rho^\beta)\, \ln\,(\rho)$$

The maximum radial stress occurs at the radial distance

$$(r)^P_{max} = \left[\frac{R_o^\beta}{2(1 - \beta)}\right]\{1 + \rho^\beta - \sqrt{[(1 + \rho^\beta)^2 + 4\rho^\beta(\beta^2 - 1)]}\}^{1/\beta}$$

(A8)

Acknowledgments

References

[1]Lagace, P. A., and Weems, D. B., "A Through-the Thickness Strength Specimen for Composites," Test Methods for Design Allowables for Fibrous Composites, edited by C. C. Chamis, Vol. 2, American Society for Testing and Materials, ASTM STP 1003, Philadelphia, PA, 1989, pp. 197–207.

[2]Sun, C. T., and Kelly, S. R., "Failure in Composite Angle Structures, Part I: Initial failure," Journal of Reinforced Plastics and Composites, Vol. 73, May 1988, pp. 220–232.

[3]O'Brien, T. K., and Salpekar, S. A., "Scale Effects on the Transverse Tensile Strength of Graphite Epoxy Composites," NASA TM 107637, June 1991.

[4]Ko, W. L., and Jackson, R. H., "Multilayer Theory for Delamination Analysis of Composite Curved Bar Subjected to End Forces and End Moments," NASA TM 4139, Sept. 1989.

[5]Ko, W. L., and Jackson, R. H., "Open-Mode Delamination Stress Concentrations in Horseshoe and Elliptic Composite Curved Bars Subjected to End Forces," NASA TM 4164, Jan. 1990.

[6]Hiel, C. C., Sumich, M., and Chappell, D. P., "A Curved Beam Test Specimen for Determining the Interlaminar Strength of a Laminated Composite," Journal of Composite Materials, Vol. 25, July 1991, pp. 854–868.

[7]Kedward, K. T., Wilson, R. S., and McLean, S. K., "Flexure of Simply Curved Composite Shapes," Composites, Vol. 20, No. 6, 1989, pp. 527–536.

[8]Martin, R. H., and Jackson, W. C., "Damage Prediction in Cross-Plied Curved Composite Laminates," Composite Materials: Fatigue and Fracture, edited by W. W. Stinchcomb and N. E. Ashbough, Vol. 4, American Society for Testing and Materials, ASTM STP 1156, Philadelphia, PA, 1993, pp. 105–125.

[9]Jackson, W. C., and Martin, R. H., "An Interlaminar Tension Strength Specimen," Symposium on Composite Materials: Testing and Design, ASTM STP 1206, edited by E. T. Camponeshi, Jr., American Society for Testing and Materials, Pittsburgh, PA, May 1993, pp. 333–354.

[10]Lekhnitskii, S. G., Anisotropic Plates, Gordon & Breach, New York, 1968, Chap. 3.

[11]Allen, H. G., "Measurement of Through-the-Thickness Strength of Laminated and Braided Composites," M.S. Thesis, Dept. of Mechanical Engineering, North Carolina A&T State Univ., Greensboro, NC, 1993.

[12]Crews, J. H., Jr., Shivakumar, K. N., and Raju, I. S., "Strain Energy Release Rate Distribution for Double Cantilever Beam Specimens," AIAA Journal, V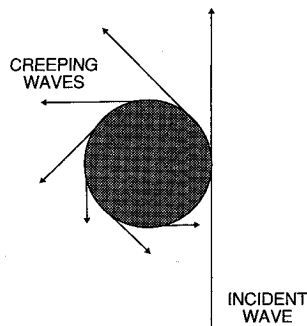ol. 29, No. 10, 1991, pp. 1686–1691.